

Inhibition fields for phyllotactic pattern formation: a simulation study¹

Richard S. Smith, Cris Kuhlemeier, and Przemyslaw Prusinkiewicz

Abstract: Most theories of phyllotaxis are based on the idea that the formation of new primordia is inhibited by the proximity of older primordia. Several mechanisms that could result in such an inhibition have been proposed, including mechanical interactions, diffusion of a chemical inhibitor, and signaling by actively transported substances. Despite the apparent diversity of these mechanisms, their pattern-generation properties can be captured in a unified manner by inhibition fields surrounding the existing primordia. In this paper, we introduce a class of fields that depend on both the spatial distribution and the age of previously formed primordia. Using current techniques to create geometrically realistic, growing apex surfaces, we show that such fields can robustly generate a wide range of spiral, multijugate, and whorled phyllotactic patterns and their transitions. The mathematical form of the inhibition fields suggests research directions for future studies of phyllotactic patterning mechanisms.

Key words: morphogenesis, spiral, whorl, inhibition, modeling, visualization.

Résumé : La plupart des théories phyllotaxiques sont basées sur l'idée que la formation de nouveaux primordiums est inhibée par la proximité de primordiums plus âgés. On a proposé plusieurs mécanismes qui pourraient conduire à une telle inhibition, incluant des interactions mécaniques, la diffusion d'un inhibiteur chimique, et une signalisation par des substances activement transportées. En dépit de la diversité de ces mécanismes, les propriétés de leur patron de développement peuvent être perçues de manière unifiée, par des champs d'inhibition autour des primordiums existants. Les auteurs proposent une classe de champs qui dépend à la fois de la distribution spatiale et de l'âge des primordiums préalablement formés. À l'aide de techniques courantes pour créer des surfaces apicales en croissance géométriquement réalistes, les auteurs montrent que de tels champs peuvent générer, de façon robuste, un large ensemble de patrons phyllotactiques spiralés, multijugués et verticillés ainsi que leurs transitions. La forme mathématique des champs d'inhibition suggère des directions de recherche pour de futures études des mécanismes sous-jacents aux patrons phyllotactiques.

Mots clés : morphogénèse, spirale, verticille, inhibition, modélisation, visualisation.

[Traduit par la Rédaction]

Introduction

Few patterns in nature are more conspicuous than the intersecting spirals of florets in a sunflower head or scales on a pine cone. These arrangements, known as phyllotactic patterns, have fascinated both mathematicians and biologists for centuries. Although much of the early literature on phyllotaxis was limited to a descriptive characterization of phyllotactic patterns, hypotheses on the underlying developmental mechanisms began to appear as long as 140 years ago.

The original hypothesis was from Hofmeister (1868), who proposed that a new primordium appears as far as possible from the edges of existing primordia. Experimental evidence supporting this assertion was provided by Snow and Snow (1931) and more recently by Reinhardt et al. (2005).

The postulate that existing primordia inhibit the formation of new primordia nearby is fundamental to most mechanistic theories of phyllotaxis, as reviewed by Schwabe (1984), Jean (1994), and Adler et al. (1997). The specific mechanisms considered include contact pressure (Schwendener 1878), diffusion of an inhibitor (Schoute 1913), reaction-diffusion (Turing 1952), surface buckling (Green 1992), and the polar transport and depletion of an activator (Reinhardt et al. 2003).

Despite the diversity of the proposed mechanisms, they share the notion of an inhibition field surrounding pre-existing primordia. This general notion raises two types of questions: (i) What molecular-level processes may produce such inhibition fields? and (ii) What is the relationship between spatial and temporal properties of the inhibition fields and the generated patterns?

In this paper, we use computer simulations to address the second question. Our objective is to find inhibition field functions that satisfy the following criteria: (i) the model can generate a wide variety of phyllotactic patterns, (ii) patterns can start de novo in an empty peripheral zone or from one or two cotyledons, (iii) the model can capture transitions in phyllotaxis, such as the often-observed transition from decussate to spiral patterns (Wardlaw 1968), and (iv) the patterns can be initiated and propagated in a robust manner. This last criterion implies, in particular, (a) low sensitivity

Received 26 April 2006. Published on the NRC Research Press Web site at <http://canjbot.nrc.ca> on 8 February 2007.

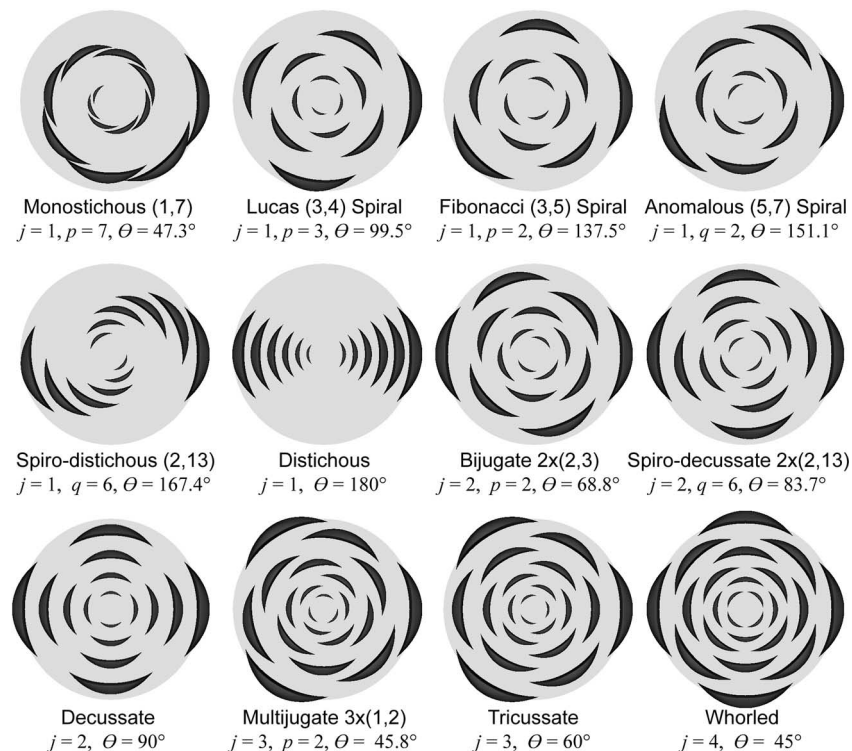
R.S. Smith and P. Prusinkiewicz.² Department of Computer Science, University of Calgary, 2500 University Drive NW, Calgary, AB T2N 1N4, Canada.

C. Kuhlemeier. Institute of Plant Sciences, University of Berne, CH-3013 Berne, Switzerland.

¹This article is one of a selection of papers published on the Special Theme of Shoot Apical Meristems.

²Corresponding author (e-mail: pwp@cpsc.ucalgary.ca).

Fig. 1. Sample phyllotactic patterns arranged by jugacy j and divergence angle θ . For spiral patterns, numbers of opposed parastichies are given in parentheses. Integers p and q characterize families of parastichies for normal and anomalous phyllotaxis, respectively, corresponding to Fibonacci-like sequences defined in the text.



to changes in the model parameter values, (b) tolerance to low cell counts in the peripheral zone, limiting the precision in which individual primordia can be placed, and (c) tolerance to random factors (noise) that may affect the placement of individual primordia.

We also require that the inhibition functions depend on distance and time in a physically plausible manner, although we do not hypothesize on specific molecular-level processes that may yield these functions. We limit our discussion to models in which the angular position of primordia does not change over time. This is consistent with the current experimentally based view of phyllotaxis (Reinhardt et al. 2003). Simulation analysis of the contact-pressure mechanism (Schwendener 1878; Adler 1974) that relies on such motions is presented in Ridley (1982) and Hellwig et al. (2006). Furthermore, we do not consider secondary changes in the angles between plant organs that may occur as they develop from primordia, for example, as a result of uneven growth at different sides of the organs.

Previous simulation models have been focused on formulas derived from a particular proposed mechanism, the diffusion of an inhibiting substance being the most common (Hellendoorn and Lindenmayer 1974; Thornley 1975; Veen and Lindenmayer 1977; Mitchison 1977; Young 1978; Meinhardt 1982, 2003; Schwabe and Clewer 1984; Chapman and Perry 1987; Yotsumoto 1993). In a steady-state approximation of the effect of a diffusing substance (Thornley 1975; Mitchison 1977; Young 1978; Yotsumoto 1993), the inhibiting influence of each primordium decreases exponentially with distance. In a system containing n pri-

mordia, their combined effect h on a sampling point S is thus calculated as the sum

$$[1] \quad h(S) = \sum_{i=1}^n e^{-bd(P_i, S)}$$

where $d(P_i, S)$ is the distance between primordium P_i and a sampling point S on the apex surface and b controls the rate of exponential decrease in inhibition with the distance from the primordium.

A different equation, motivated by physical experiments in which phyllotactic patterns were generated in a magnetic field, was proposed by Douady and Couder (1992, 1996a, 1996b, 1996c). With this formula, inhibition decreases with the distance from the source according to the power function

$$[2] \quad h(S) = \sum_{i=1}^n \frac{1}{d(P_i, S)^b}$$

where $d(P_i, S)$ is defined as in eq. 1 and b controls the rate of inhibition decrease with the distance from a primordium.

Equations 1 and 2 can generate phyllotactic patterns, yet in our simulations, they showed limitations: we were not able to find parameters needed to reproduce some patterns, such as higher order accessory patterns ($p > 6$, see below for terminology), while other patterns and their transitions only occurred in very narrow ranges of parameter values. These limitations are difficult to quantify because of the number of parameters involved: the results of simulations depend not only on the inhibition fields under investigation

but also on the assumed shape of the apex, its growth pattern, the position of the peripheral zone, the initial distribution of primordia, and the manner in which all of these characteristics and parameters change over time. Nevertheless, in a series of interactive experiments with simulation models, we found that robust de novo generation of a variety of phyllotactic patterns and their transitions was much easier when the inhibition fields depended both on the spatial arrangement of existing primordia and on their age. Below, we describe the specific fields used and the results of our simulation experiments.

Materials and methods

Terminology

We describe the arrangement of organ primordia on the growing surface of the apex (Fig. 1) using the terminology based on (Jean 1994). The term whorl size or jugacy, denoted j , is used to specify the number of primordia emerging simultaneously. If primordia are issued one at a time ($j = 1$), the pattern is unijugate. For unijugate patterns, the divergence angle is defined as the angle between consecutive primordia. The vertex of this angle lies on the longitudinal axis of the apex. If the divergence angle is equal to 180° , the phyllotactic pattern is distichous; otherwise, it is spiral. The latter term reflects the shape of conspicuous lines, or parastichies, formed by neighboring organs. Typically, there are two sets of intersecting spiral parastichies, running in opposite directions. The number of parastichies is a distinctive feature of the pattern. In Fibonacci patterns, the numbers of opposite parastichies are consecutive elements of the Fibonacci sequence $\langle 1, 2, 3, 5, 8, 13, 21, \dots \rangle$. The first two elements of this sequence are equal to 1, and each successive element is the sum of two previous elements. In the more general case of Fibonacci-like sequences, each successive element is still equal to the sum of previous ones, but the first two elements are different. A sequence $\langle 1, p, p + 1, 2p + 1, 3p + 2, 5p + 3, \dots \rangle$ with $p > 2$ is termed the $(p - 2)$ th accessory sequence. The first accessory sequence $\langle 1, 3, 4, 7, 11, \dots \rangle$ is also called the Lucas sequence. An anomalous sequence is of the form $\langle 2, 2q + 1, 2q + 3, 4q + 4, 6q + 7, \dots \rangle$, where $q > 1$. In multijugate patterns, the numbers of parastichies are multiples of those found in the underlying unijugate spiral patterns. For example, in a bijugate Fibonacci pattern ($j = 2$), the numbers of opposite parastichies are consecutive elements of the sequence $2 \times \langle 1, 2, 3, 5, 8, 13, 21, \dots \rangle$. Patterns with the parastichy numbers being consecutive elements of the same sequence are of the same type. Within a type, a pattern with a higher number of parastichies is said to have a higher order. In contrast with the multijugate patterns, in whorled patterns, new primordia appear in the centers of the spaces between primordia of the previous whorl. Whorled patterns with the whorl size equal to 2 or 3 are termed decussate and tricussate patterns, respectively. In the case of multijugate and whorled patterns, the divergence angle is defined as the smallest angle between primordia in successive whorls.

Each phyllotactic pattern can only occur if the divergence angle lies within some interval, which we call the allowable

interval for this pattern. For each family of patterns (e.g., Fibonacci or Lucas patterns), the bounds of this interval tend to a limit value, called the limit divergence angle, as the order of the pattern increases. Equations for the bounds of intervals and limit divergence angles for typical phyllotactic patterns are presented in Jean (1994, pp. 36–38).

Geometric model of a growing apex

We model the shoot apical meristem as a surface of revolution generated by rotating a planar curve around the longitudinal axis of the apex (Fig. 2) (Smith et al. 2006). This planar curve is a B-spline (Foley et al. 1990) defined interactively using a graphical editor and can easily be changed to model apices with various profiles of their central longitudinal sections. A point P on the apex surface is represented by two coordinates (θ, a) , where θ is the angle of rotation around the axis of the apex, measured with respect to a reference direction, and a is the distance from the apex tip, measured along the generating curve on the apex surface. In Cartesian coordinates, the position of point P is thus given by

$$[3] \quad (x, y, z) = (x_a(a)\cos(\theta), y_a(a), x_a(a)\sin(\theta))$$

We assume that individual points move away from the apex tip as a result of growth, although the overall shape of the apex does not change. This motion is characterized by a function $\text{RERG}(a)$ (Richards and Kavanagh 1943; Erickson and Sax 1956; Hejnowicz and Romberger 1984), which defines the relative elementary rate of growth in the longitudinal direction (along the generating curve) at a distance a from the apex tip (Hejnowicz et al. 1984; Nakielski 2000; Smith et al. 2006). The velocity with which a point $P = (\theta, a)$ moves away from the apex tip along the generating curve is then given by the integral

$$[4] \quad v(a) = \int_0^a \text{RERG}(a) da$$

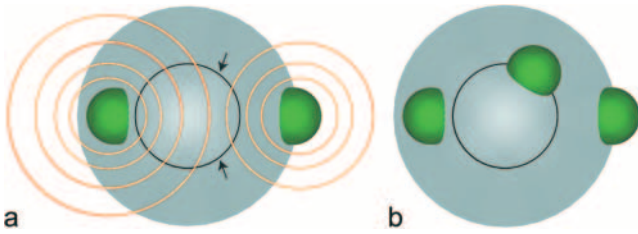
Similar to the generating curve, the growth function $\text{RERG}(a)$ is defined graphically, which makes it easy to specify various distributions of growth on the surface of the apex. Two RERG functions used in the simulations are shown in Fig. 3. The generated patterns did not depend critically on the choice of the RERG function.

The shoot apical meristem consists of a central zone of undifferentiated founder cells surrounded by a relatively narrow band of cells called the peripheral zone (Steeves and Sussex 1989; Lyndon 1998). As the plant develops, the peripheral zone maintains an approximately constant distance from the tip of the apex. Only cells within the peripheral zone are competent to initiate organs. In our simulations, we assumed that the growth was slower in the central zone than in the peripheral zone, as suggested by experimental data (Lyndon 1998). New primordia appear on the active ring, which we define as a circle situated in the middle of the peripheral zone (Fig. 2).

Organization of computation

Our simulation models are based on the idea that the existing primordia exert an inhibiting influence on the incipient primordia (Fig. 4). The combined influence of all

Fig. 4. Diagram of inhibition. (a) The older primordium has a smaller inhibiting effect on the active ring than the newer primordium. Arrows indicate minima of inhibition where a new primordium can appear. (b) The upper minimum of inhibition was chosen as the location of the third primordium.



ring as a result of the apex growth. This movement, combined with a possible decrease of the inhibiting influences of primordia with their age, reduces the inhibiting field strength on the active ring. Over time, this inhibition drops sufficiently at some location to allow for the formation of another primordium, and the process repeats.

Software implementation

The simulation models have been implemented using the modeling software *vv* (Smith et al. 2003), which extends the C++ programming language with constructs for modeling spatial systems with a dynamically changing structure.

Results

Single inhibition function

The first simulation model discussed uses a single inhibition function. In an apex with n previously formed primordia, the total inhibiting effect $h(S)$ of previous primordia is calculated as the sum

$$[5] \quad h(S) = \sum_{i=1}^n \frac{1}{d(P_i, S)} e^{-bt_i}$$

where $d(P_i, S)$ is defined as in eq. 1, t_i is the age of primordium i , and b controls the rate of exponential decrease in inhibition over time. The essential feature of this formula is the explicit dependence of the field on both the distance from the primordia and their age. We found that the specific form of the distance dependence is not critical, although the inversely proportional function suggested by eq. 2 leads to slightly more robust results than the exponential dependence suggested by eq. 1. Note that, according to eq. 5, the unit value of inhibition h is defined as that produced by a newly formed primordium ($t_i = 0$) at the unit distance from the primordium center ($d(P_i, S) = 1$).

We examined the pattern-generating capability of the model generated with the inhibition function [eq. 5] from two perspectives: generation of patterns *de novo* (including generation of sequences of patterns, with transitions caused by changes in parameter values) and perpetuation (maintenance) of patterns initiated with a sequence of preplaced primordia.

Pattern generation *de novo*

In these simulations, no primordia, and thus no inhibition field, were present at the beginning of the simulation. The

generating algorithm located the first primordium at a random position on the active ring (simulations with a predefined position of the initial primordium produced the same results). Simulations with high initial values of the inhibition threshold often produced apparently unorganized arrangements of primordia, before settling into a pattern. To prevent these unorganized arrangements from occurring while focusing on the biologically relevant situation where patterns begin with the arrangement of cotyledons, the inhibition threshold value was phased in gradually, increasing from an initial value of zero to the final value used in the simulation. This increase led to transitions in the phyllotaxis type or order.

For example, in the simulation shown in Fig. 6, the initial value of the threshold for primordium differentiation was relatively low, yielding a distichous pattern. After an increase in the threshold value, a spiro-distichous pattern emerged. Continued increases in the threshold value caused a switch to Fibonacci spiral phyllotaxis. Similar progression of patterns could be obtained when changing the size of the apex while keeping the threshold value constant. This is relevant from the biological perspective, since changes in the apex size are known to correlate with changes in the patterns (Kwiatkowska and Florek-Marwitz 1999).

The simulation in Fig. 7 was performed using 38 sampling points on the active ring; this number was chosen to be comparable with the number of cells around the peripheral zone of an *Arabidopsis* vegetative shoot apex (cf. Fig. 2 in Kwiatkowska 2006). Furthermore, the increase in the inhibition threshold was faster than in the previous example. Under these conditions, the model produced a sequence of divergence angles that are within the standard error of angles measured during the initial establishment of a spiral pattern in *Arabidopsis* (Fig. 8).

Pattern propagation

Owing to various factors, such as the influence of cotyledons on the initial state of the simulation, limited accuracy of primordium placement caused by the relatively small number of cells around the circumference of the peripheral zone, or random factors (noise), an initial pattern of primordia positions may be different from that obtained in self-starting simulations described above. Consequently, perpetuation of such patterns is also of biological interest. We investigated the perpetuation of patterns by initiating the simulation with a number of primordia placed at the limit divergence angle characteristic to a given pattern type.

The model based on eq. 5 robustly perpetuated all of the phyllotactic patterns commonly observed in nature in which primordia appear one at a time. This includes distichous and spiro-distichous as well as Fibonacci, Lucas, and anomalous spiral patterns. In all simulations, the opposing parastichy numbers were consecutive numbers of some Fibonacci-like sequence. High-order patterns, such as (89, 144) Fibonacci spirals, could be perpetuated if the number of sampling points in the active ring was sufficiently large to represent a divergence angle within the allowable interval for the given pattern (the size of this interval decreases as the order of the pattern increases). Occasionally, however, regular phyllotactic patterns could be generated even when the number of

Fig. 5. Dynamics of interaction between the inhibiting field and phyllotactic pattern formation. The field was calculated using eq. 5. (a) The field generated by two symmetrically placed initial primordia. (b) The field shortly before the insertion of the third primordium. Arrows indicate minima of the inhibition field. The location indicated by the black arrow is chosen at random over the location indicated by the grey arrow as the location of the third primordium. (c–e) The field before the insertion of the fourth, fifth, and sixth primordium. (f–h) The steady-state dynamics of the inhibiting field. (f) The field immediately after the insertion of primordium n . (g) The field immediately before the insertion of primordium $n + 1$. At the time of insertion of primordium $n + 1$ (longest arrow), approximate positions of incipient primordia $n + 2$ and $n + 3$ are already visible as smaller local minima of the inhibition field (shorter arrows). (h) The field immediately after the insertion of primordium $n + 1$. Note that Figs. 5f and 5h differ only by rotation of approximately 137.5° .

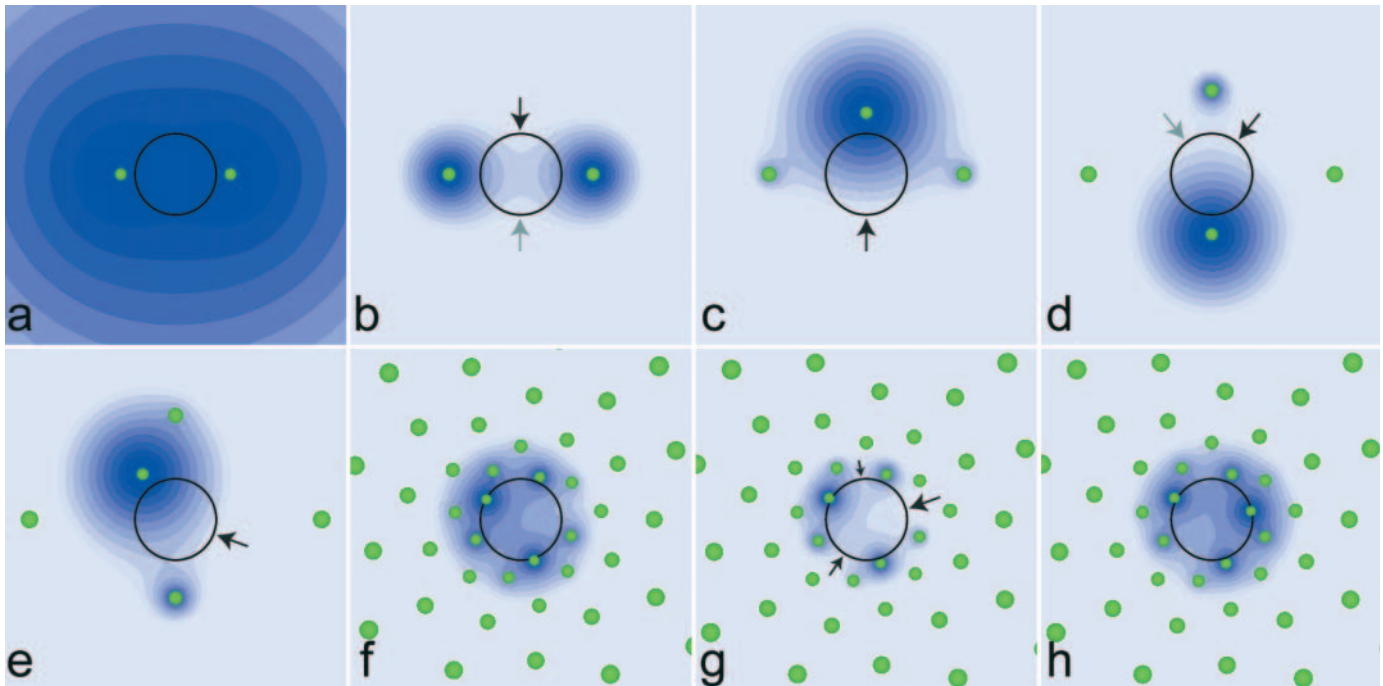


Table 1. Minimum values of the inhibition threshold needed to maintain selected phyllotactic patterns.

Phyllotaxis type	Jugacy	Sequence	Divergence angle ($^\circ$)	Min. threshold
Fibonacci	1	1, 2, 3, 5, 8, 13, ...	137.51	4
Lucas	1	1, 3, 4, 7, 11, 18, ...	99.50	22
Bijugate	2	2, 4, 6, 10, 16, ...	68.76	31
Anomalous	1	2, 5, 7, 12, 19, 31, ...	151.14	37
Other	1	3, 7, 10, 17, 27, ...	106.45	65
Second accessory	1	1, 4, 5, 9, 14, 23, ...	77.86	128

Note: See data pertinent to Fig. 9 in Appendix A for the remaining parameter values.

sampling points was smaller; in these cases, the divergence angle would oscillate and its average value would lie within the bounds (see the discussion of pattern robustness for an example).

In a series of simulation experiments, we observed that Fibonacci spiral patterns were perpetuated under the widest range of model parameter values followed by Lucas patterns and patterns from other Fibonacci-like sequences. This is consistent with observations in nature, where most single spiral patterns come from the Fibonacci, the Lucas, or the $\langle 2, 5, 7, 12, \dots \rangle$ anomalous sequence (Zagórska-Marek 1985; Jean 1994). Table 1 shows the minimum values of the inhibition threshold for which these patterns can be perpetuated, assuming constant values of other parameters. There is no maximum value of this threshold, as it can be

raised indefinitely, yielding a sequence of patterns of increasingly high orders.

Table 1 indicates that if the inhibition threshold is greater than or equal to 128, six different patterns can be propagated depending on the placement of initial primordia. These patterns are illustrated in Fig. 9. The possibility of propagating such a wide variety of patterns for the same parameter values was an unexpected result of simulations and it may explain why different types of phyllotaxis may occur in the same species: if the initial placement of primordia is affected by random factors, different patterns may emerge and be perpetuated. For example, causal observation of pine cones collected from the trees on the University of Calgary campus indicated that they usually had Fibonacci spiral phyllotaxis, but many of them had Lucas spiral phyllotaxis, and

Fig. 6. Effects of changes in inhibition threshold. At low inhibition thresholds, a self-starting distichous phyllotaxis is produced. Increases in the threshold values cause a switch to spiro-distichous and then to spiral Fibonacci patterns.

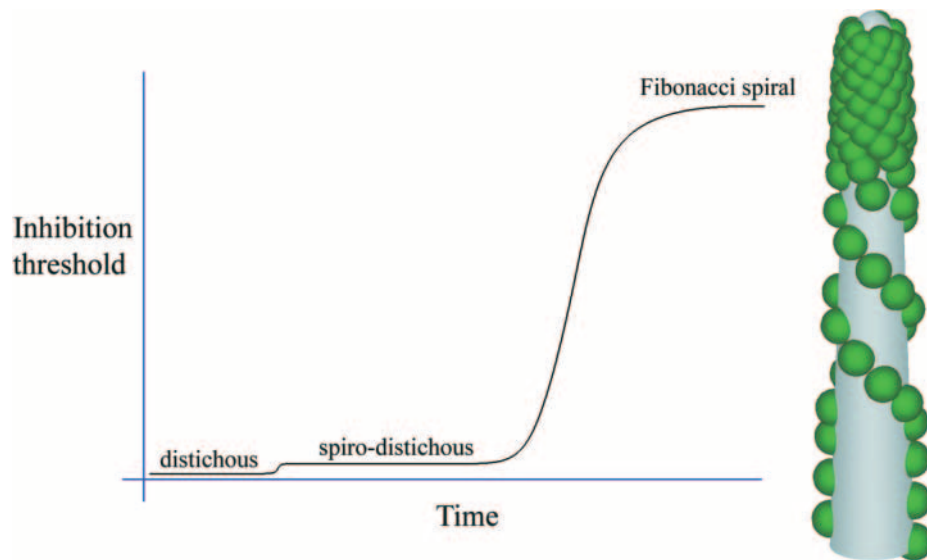
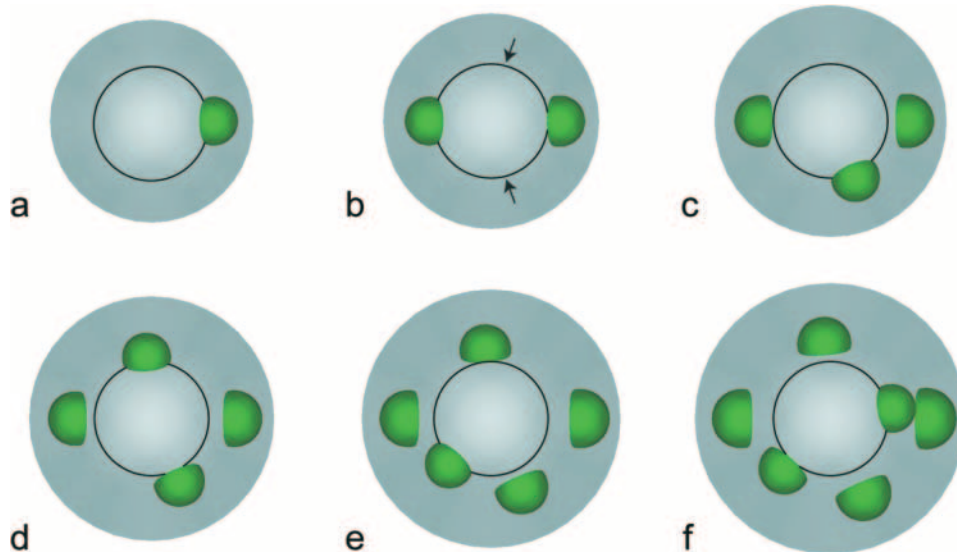


Fig. 7. Self-starting spiral Fibonacci pattern created by using an active ring with 38 sampling points. (a) The initial primordium is arbitrarily placed by the model. (b) The second primordium appears in the area of least inhibition at a divergence angle of 180° from the first. At this point, there are two minima of inhibition on the active ring, both of which are closer to the older of the two existing primordia (arrows). (c) The third primordium appears at one of these minima with a divergence angle of 114° , the choice determining the direction of the spiral. (d-f) Successive divergence angles of 161° , 133° , and 142° ensue. The model will then continue at 142° generating (3, 5) spiral phyllotaxis.



the two types often coexisted on the same tree. Flowers and inflorescences with a wide range of phyllotactic patterns were observed, for example, in *Magnolia* by Zagórska-Marek (1994), in *Helianthus annuus* L. by Couder (1998), and in Araceae by Jean and Barabé (2001).

The number of initials required to start a pattern varied considerably. While patterns from the main Fibonacci sequence were easily generated de novo, Lucas patterns required at least three initials. Patterns derived from accessory sequences with $n > 3$ could also be propagated but required a higher number of carefully placed initial primordia. For example, 40 initials placed at 64.08° were required to maintain (11, 17) phyllotaxis derived from the third accessory sequence ($n = 5$). An anomalous (7, 12) pattern could be

started with as few as six initials placed at the angle 151.14° . These high numbers of initial primordia indicate that the inhibiting fields required to propagate the corresponding patterns may emerge in nature (for example, due to a confluence of random factors), but the probability is small. This is consistent with Jean's (1994) summary of frequency data, indicating that phyllotactic patterns derived from various accessory and anomalous sequences occur in nature, but are rare.

Once a low-order spiral pattern is established, an increase in the inhibition threshold can result in the pattern switching to higher orders of phyllotaxis. This occurs for Fibonacci spiral patterns as well as patterns from accessory and anomalous sequence, provided that the increase is not sudden and

Fig. 8. Comparison of simulation model with measured divergence angles of *Arabidopsis* (Smith et al. 2006) for the first 10 primordia. The active ring has 38 sampling points, which limits the accuracy of the placement of primordia to 9.5° increments.

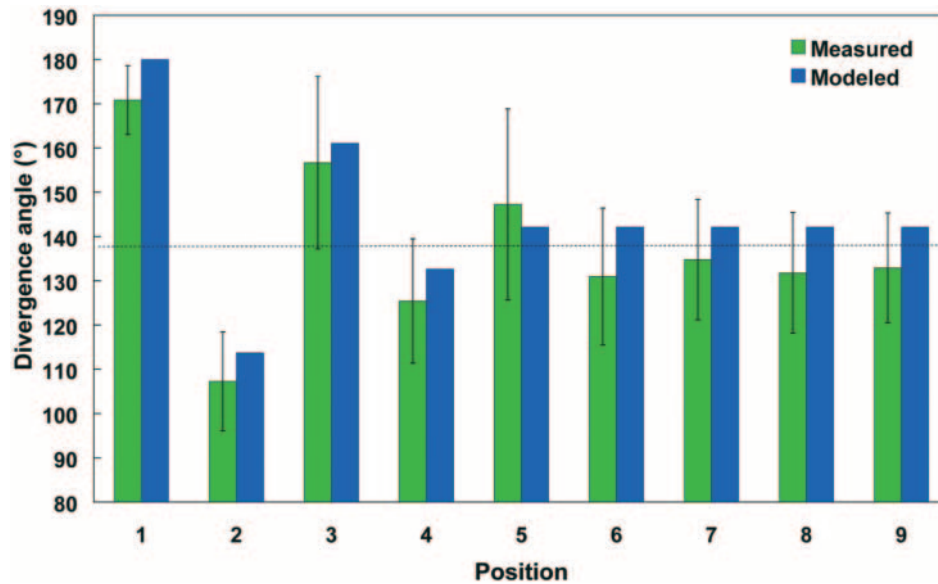
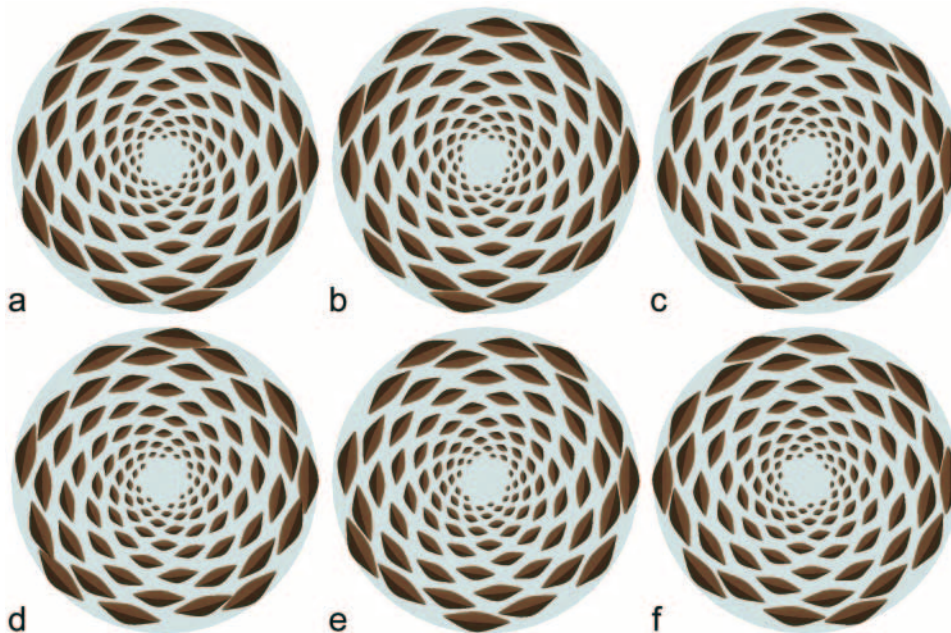


Fig. 9. Different patterns propagated using the same parameter values. These simulations differ only by the divergence angle θ between the 20 initial primordia. (a) $\theta = 77.96^\circ$ yields a second accessory (9, 14) spiral pattern; (b) $\theta = 99.50^\circ$ yields a Lucas (7, 11) spiral pattern; (c) $\theta = 106.4^\circ$ yields a (7, 10) spiral pattern; (d) $\theta = 137.51^\circ$ yields a Fibonacci (8, 13) spiral pattern; (e) $\theta = 151.14^\circ$ yields an anomalous (7, 12) spiral pattern; (f) $\theta = 68.76^\circ$ and jugacy $j = 2$ yields a bijugate (6, 10) spiral pattern.



the number of sampling points on the active ring is large enough to support the higher order pattern. Sharp increases in inhibition threshold in accessory and anomalous patterns produce less predictable results. In some cases, the pattern would become disorganized. In others, a switch to a Fibonacci spiral phyllotaxis was observed. Stable, although not very regular, bijugate patterns were often generated as well. Parastichy numbers produced by these patterns were always a multiple ($\times 2$) of consecutive elements of the Fibonacci sequence.

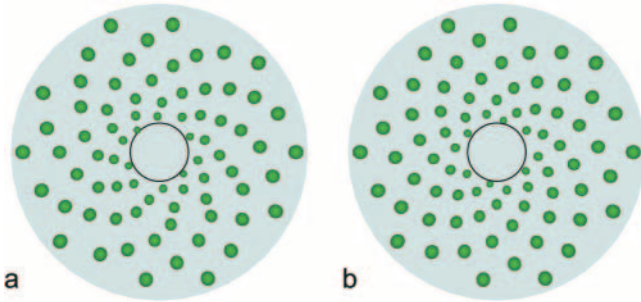
In bijugate patterns, pairs of primordia are expected to appear simultaneously, yet in the above simulations, this is not the case. The first primordium of each pair has an immedi-

ate inhibiting effect on the entire ring, which delays the appearance of the second primordium. As a result of this delay, the bijugate patterns are slightly irregular (Fig. 10).

Two inhibition functions

In general, the single-inhibitor model characterized by eq. 5 is not suitable for generating patterns in which two or more primordia appear simultaneously. Figure 11 illustrates this limitation by using a decussate pattern as an example. Suppose the first two primordia have been placed 180° apart, and the inhibition levels at the entire active ring are too high for additional primordia to appear. Over time, the

Fig. 10. Examples of bijugate $2 \times (5, 8)$ patterns. (a) The pattern generated using the single-inhibitor model. Although parastichies are clearly visible, the positioning of individual primordia is slightly irregular due to the delay in the production of the second primordium in each pair. (b) The regular pattern generated by the variant of the single-inhibitor model with explicitly imposed jugacy. The pattern generated by the two-inhibitor model is similar.



inhibiting effect of these initial primordia decreases as a result of apex growth, and two identical inhibition minima appear in a perpendicular orientation on the active ring (Fig. 11a). When the inhibition level at these minima falls below the threshold, one minimum is selected by the placement algorithm as the location of the third primordium (Fig. 11b). The immediate inhibiting influence of this primordium pushes the other minimum above the threshold, delaying the appearance of the fourth primordium until the apex grows further (Fig. 11c). As a result, the third primordium has a weaker inhibiting effect on the active ring than the more recently formed fourth primordium, and the fifth primordium is positioned asymmetrically (Fig. 11d), causing a switch to spiral phyllotaxis.

We implemented a variant of the single inhibition model in which jugacy j is specified as a model parameter. Inhibition is calculated with eq. 5, considering possible positions of j evenly spaced locations on the active ring. When the sum of inhibitions at these locations drops below the inhibition threshold, j primordia are placed simultaneously. With this strategy, the model is able to robustly produce decussate, whorled, bijugate, and multijugate patterns. However, the assumed placement algorithm is difficult to justify in mechanistic terms.

The inability of the model summarized by eq. 5 to create patterns in which two or more primordia appear at once is a consequence of two factors: (i) the spatially unlimited inhibiting influence of each primordium and (ii) the immediate effect of each primordium on the entire active ring. In reality, it is unlikely that the full inhibiting effect of a primordium will be felt the instant a primordium appears. This is especially true for sampling points located some distance away from the new primordium. To delay the inhibiting effect, we introduced two modifications to the model. First, the inhibiting influence of a primordium on the active ring is phased in gradually using the following modification of eq. 5:

$$[6] \quad h_1(S) = (1.0 - e^{-b_d t_i}) \sum_{i=1}^n \frac{1}{d(P_i, S)} e^{-b_l t_i}$$

As in eq. 5, b_l is the coefficient for exponential decay of in-

hibition, $d(P_i, S)$ is the distance between sampling point S and primordium P_i , and t_i is the age of primordium P_i . The additional parameter b_d controls the rate with which the inhibiting influence of the primordium is phased in. According to eq. 6, a newly placed primordium does not immediately increase the inhibition levels at other locations, making it possible for primordia at other minima to appear concurrently. This sets the stage for the formation of whorled and multijugate patterns.

The problem with the above mechanism is that the inhibition threshold can be reached at a series of neighboring locations in quick succession, leading to the formation of closely spaced primordia. To prevent this from happening, we introduce a second inhibiting function:

$$[7] \quad h_s(S) = \sum_{i=1}^n \frac{1}{d(P_i, S)} e^{-b_s t_i}$$

where parameters $d(P_i, S)$ and t_i are as above and b_s controls the rate of exponential decay of the second inhibition over time. A new primordium is formed when both inhibiting influences are below predefined threshold values. Equation 6 is used to express long-range inhibition that determines the phyllotactic patterning of primordia, and eq. 7 is used to express short-range inhibition that prevents creation of multiple primordia at adjacent locations on the active ring. The short-range inhibition decreases over time faster than the long-range inhibition ($b_s > b_l$) and thus does not interfere with the phyllotactic positioning of primordia, which remains governed by the long-range inhibition.

Pattern generation de novo

The model with two inhibition functions (two-inhibitor model for short) can create de novo the distichous, spiro-distichous, and spiral Fibonacci patterns produced by the single inhibitor model as well as decussate, spiro-decussate, whorled, and bijugate patterns (Fig. 12). Experimenting with model parameters, we found that spiral Fibonacci patterns are generated most often, as in the case of the single-inhibitor model. In contrast with that model, however, the second most easily produced spiral patterns are bijugate patterns, with parastichy numbers being twofold multiples of the main Fibonacci sequence, $2 \times \langle 1, 2, 3, 5, 8, 13, \dots \rangle$. The next most frequently observed spiral patterns correspond to the Lucas sequence. These frequencies are consistent with the experimental data (Zagórska-Marek 1985; Jean 1994, pp. 148–151).

Many plants undergo changes in phyllotaxis during development. Transitions often occur quickly, so that a new pattern is established within the span of a few plastochrons. These transitions can be simulated using the two-inhibitor model by manipulating the long-range and short-range inhibition thresholds during simulation. For example, Fig. 13 illustrates the transition from decussate to spiral phyllotaxis, frequently observed in nature (Wardlaw 1968; Carpenter et al. 1995; Kwiatkowska 1995, 1997), and the transition from decussate to bijugate phyllotaxis. The model can also simulate other transitions, including distichous to Fibonacci spiral, whorled to Fibonacci or Lucas spiral, whorled to multijugate, and multijugate to Fibonacci spiral.

Fig. 11. Decussate patterns are not sustained because of the immediate inhibiting effect of new primordia. Arrows indicate minima of inhibition where the third primordium can appear. (*a–d*) Consecutive stages of pattern formation.

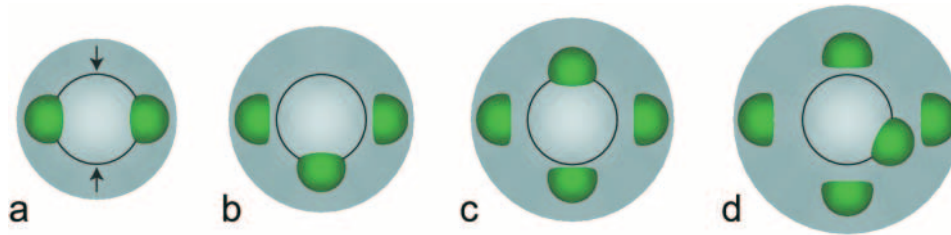
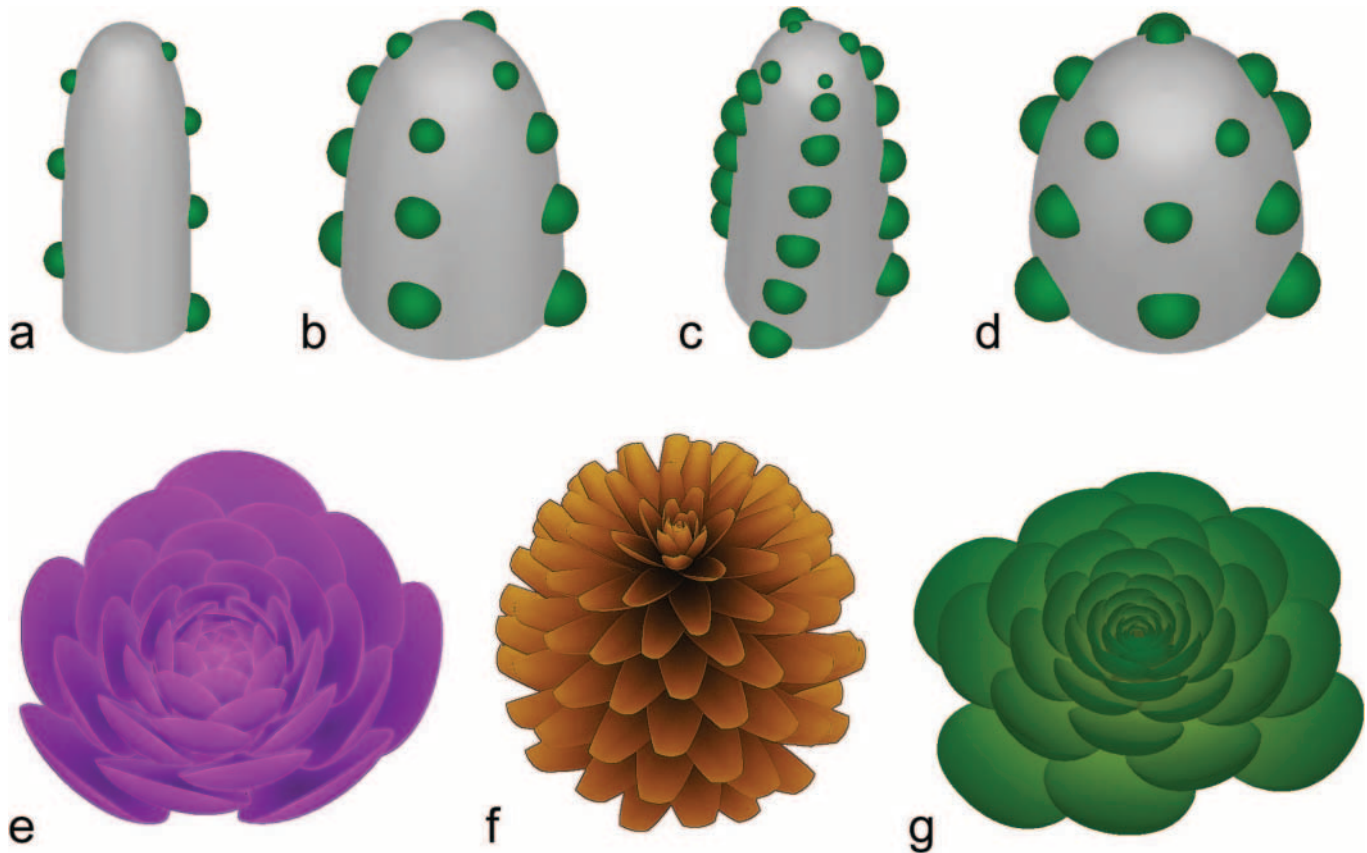


Fig. 12. Examples of phyllotactic patterns produced by the two-inhibitor model: (*a*) distichous, (*b*) decussate, (*c*) spiro-decussate, (*d*) whorled, (*e*) Fibonacci spiral, (*f*) Lucas spiral, and (*g*) bijugate. The patterns in Figs. 12*a*, 12*b*, 12*c*, 12*e*, and 12*g* have been generated de novo; the patterns in Figs. 12*d* and 12*f* have been propagated by the model from a predefined initial pattern.



Pattern propagation

The model with two inhibition functions can propagate the same patterns as the single inhibition model as well as decussate, whorled, and multijugate patterns (Fig. 12). As in the case of the single-inhibitor model, different patterns can be propagated by the model using the same parameter values. The range of patterns that can be propagated that way is surprisingly large and includes, for example, the entire inventory of single and multijugate spiral patterns reported by Zagórska-Marek (1985).

Robustness of the models

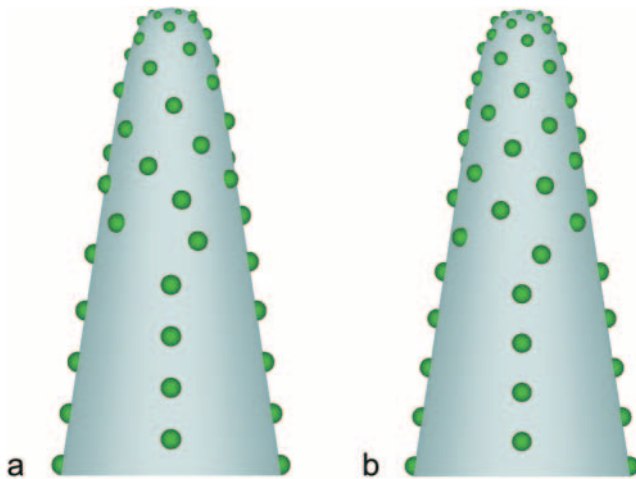
Although exceptions exist (Zagórska-Marek 1994), phyllotactic pattern formation in nature is often very robust, which means that patterns are formed or maintained under a wide range of conditions. Plausible models of phyllotaxis

should therefore generate stable patterns or sequences of patterns (including transitions) over a wide range of parameter values.

A critical parameter of the models discussed in this paper is the inhibition threshold at which new primordia are formed. Both the single-inhibitor and the two-inhibitor models produce identifiable phyllotactic patterns over a wide range of long-range inhibition thresholds. Variation of this parameter during simulation induces transitions in phyllotaxis type or order (Figs. 6 and 13).

The two-inhibitor model also includes a threshold for short-range inhibition. Values of this parameter are more critical than those of the long-range inhibition threshold. For example, in the case of decussate patterns, the short-range threshold values can only be changed by approximately $\pm 20\%$ without affecting the pattern. This sensitivity

Fig. 13. Examples of transitions in phyllotactic patterns generated by the two-inhibitor model: (a) decussate to spiral and (b) decussate to bijugate.



can be understood in the context of the role of the short-range inhibition in multijugate pattern formation: the threshold values must be low enough to effect suppression of adjacent primordia yet high enough to allow for proper positioning of other members of the whorl. The parameters b_d and b_s , which control delay of long-range inhibition and decrease of short-range inhibition over time, can be manipulated within ranges exceeding $\pm 20\%$ of the mean value.

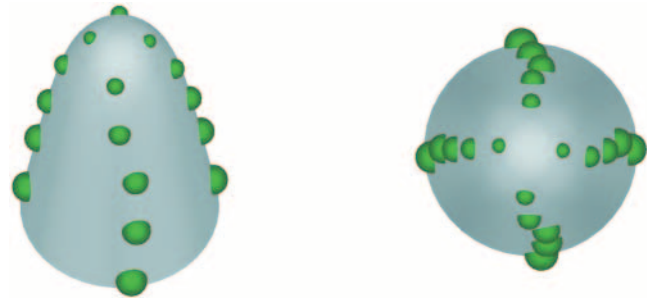
The parameter b (b_1 in the two-inhibitor model), which controls the exponential decay of inhibition with the age of primordia, also has a significant effect on pattern formation. Nonzero values of this parameter make it easier to initiate patterns de novo, allow for faster transitions between patterns, and make it possible to maintain patterns for wider ranges of apex shapes and other parameter values. On the other hand, the model is capable of generating regular phyllotactic patterns even as b or b_1 approaches zero. In this case, the inhibition exercised by a primordium [eq. 5 or 6] no longer depends on its age but decreases only with distance as in the simulations performed by Douady and Couder (1992).

Recognizable phyllotaxis (determined by examination of divergence angles) is generated for various apex shapes, such as disk, cylinder, cone, hemisphere, or arbitrary surfaces of revolution. Both the single-inhibitor and the two-inhibitor models are also robust with respect to changes in the RERG function. Nevertheless, the shape of the apex, its growth rate, the size and shape of primordia, and the number of sampling points on the active ring can have drastic effects on which parastichy pairs, if any, are clearly visible (Schwabe 1984, p. 410).

Both models are robust with respect to noise. For example, decussate phyllotaxis, which has a strong tendency to break symmetry and switch to spiral phyllotaxis, is nevertheless stable in the presence of considerable noise (Fig. 14).

The last parameter considered is the number of sampling points on the active ring. With n sampling points, the divergence angles can be represented with the resolution of $360^\circ/n$, which limits the precision with which primordia can be placed on the active ring. Low-order phyllotactic patterns can easily

Fig. 14. Side and top views of a decussate pattern simulated in the presence of noise. Sampling points on the active ring were perturbed at random in both the longitudinal and circumferential directions. Increasing the amplitude of the noise would cause a switch to spiral phyllotaxis.



be generated even for small numbers of sampling points, in the range of 10–20. Higher order patterns, or patterns from less common accessory sequences, require larger numbers of sampling points. Nevertheless, the model is robust enough to generate some high-order patterns even for relatively small numbers of sampling points. For example, an active ring with 19 sampling points makes it possible to represent divergence angles with the resolution of $360^\circ/19 \approx 18.9^\circ$. The closest two angles to the limit Fibonacci angle of 137.5° are $7 \times (360^\circ/19) \approx 132.6^\circ$ and $8 \times (360^\circ/19) \approx 151.6^\circ$. Both of these angles are outside the allowable interval $[135^\circ, 144^\circ]$ of divergence angles for (5, 8) spiral phyllotaxis. Nonetheless, the model can create a rough (5, 8) spiral pattern by alternating between 132.6° and 151.6° as follows: $151.6^\circ-132.6^\circ-132.6^\circ-151.6^\circ-132.6^\circ-132.6^\circ-151.6^\circ\dots$. The average divergence angle over many primordia is 138.9° , which lies within the interval $[135^\circ, 144^\circ]$.

Discussion

Phyllotaxis is an example of an emergent phenomenon in which properties of the whole pattern result from interactions between individual elements of the pattern, yet the causal link between these interactions and the pattern is not obvious. For this paper, we investigated the inhibiting effect that the existing primordia may have on the placement of new primordia when generating the observed phyllotactic patterns and their transitions. We found that (i) a wide class of patterns can be robustly generated de novo or indefinitely propagated if the inhibiting effect of an existing primordium depends both on the age of a primordium and on the distance between the primordium and a point on the apex, (ii) different phyllotactic patterns can be propagated by models using the same simulation parameters, (iii) multijugate and whorled patterns, in which two or more primordia appear at once, can be robustly generated if the inhibiting effect of each primordium is not immediate, but gradually phased in, and (iv) an additional short-range inhibiting mechanism is then needed to prevent formation of series of primordia in neighboring locations.

We summarized the cumulative impact of existing primordia on the apex of a field that assigns a value of the inhibition to each point on the apex. The inhibition field represents a useful level of abstraction, which makes it

possible to analyze and visualize the dynamics of interactions between primordia without knowing the specific mechanism by which these interactions are implemented in nature. Nonetheless, general properties of the inhibition field point to the properties that a molecular-level mechanism may have to produce these patterns. For example, simulations suggest that an optimal contribution of a primordium to the field decreases with the inverse of distance. Such a decrease does not need to be of a diffusion-decay type postulated in several earlier models (Thornley 1975; Mitchison 1977; Young 1978; Yotsumoto 1993). This is consistent with the current view that active transport of auxin plays an important role in the formation of phyllotactic patterns (Reinhardt et al. 2003; Smith et al. 2006; Jönsson et al. 2006).

We also observed that the simulation models initiate patterns more easily, are capable of effecting more rapid transitions, and are generally more robust when the inhibiting field depends on the age of primordia. This is consistent with the idea that the differentiation and growth of primordia may have a direct impact on the phyllotactic patterns. Furthermore, short-range inhibition is required to form multijugate and whorled patterns in the model. Such a mechanism may be related to the establishment of organ boundaries and organ separation in nature. These properties of our model are consistent with the molecular-level model of phyllotaxis proposed by Smith et al. (2006), which required the introduction of primordium differentiation and organ boundaries to simulate the observed phyllotactic patterns.

Acknowledgements

Our work on the modeling of phyllotaxis on growing apices has been inspired by preliminary results obtained by Dr. Johannes Battjes during his postdoctorate fellowship at the University of Calgary. We thank Dr. Colin Smith (University of Calgary) for developing the modeling software vv and Dr. Beata Zagórska-Marek (University of Wrocław, Poland) and Brendan Lane (University of Calgary) for critical reading of the manuscript. This work was supported by the Natural Sciences and Engineering Research Council of Canada (NSERC) and Informatics Circle of Research Excellence (iCORE) postgraduate scholarships (to R.S.S.), Swiss National Science Foundation grant 3100A0-105807 (to C.K.), and Human Frontier Science Program research grant RGP0013_2001 and NSERC discovery grant RGP 130084 (to P.P.).

References

- Adler, I. 1974. A model of contact pressure in phyllotaxis. *J. Theor. Biol.* **45**: 1–79. doi:10.1016/0022-5193(74)90043-5. PMID:4836880.
- Adler, I., Barabé, D., and Jean, R.V. 1997. A history of the study of phyllotaxis. *Ann. Bot. (Lond.)*, **80**: 231–244.
- Carpenter, R., Copsey, L., Vincent, C., Doyle, S., Magrath, R., and Coen, E. 1995. Control of flower development and phyllotaxy by meristem identity genes in *Antirrhinum*. *Plant Cell*, **7**: 2001–2011. doi:10.1105/tpc.7.12.2001. PMID:8718618.
- Chapman, J.M., and Perry, R. 1987. A diffusion model of phyllotaxis. *Ann. Bot. (Lond.)*, **60**: 377–389.
- Couder, Y. 1998. Initial transitions, order and disorder in phyllotactic patterns: the ontogeny of *Helianthus annuus*. A case study. *Acta Soc. Bot. Pol.* **67**: 129–150.
- Douady, S., and Couder, Y. 1992. Phyllotaxis as a physical self-organized process. *Phys. Rev. Lett.* **68**: 2098–2101. doi:10.1103/PhysRevLett.68.2098. PMID:10045303.
- Douady, S., and Couder, Y. 1996a. Phyllotaxis as a dynamical self organizing process. Part I: The spiral modes resulting from time-periodic iterations. *J. Theor. Biol.* **178**: 255–274. doi:10.1006/jtbi.1996.0024.
- Douady, S., and Couder, Y. 1996b. Phyllotaxis as a dynamical self organizing process. Part II: The spontaneous formation of a periodicity and the coexistence of spiral and whorled patterns. *J. Theor. Biol.* **178**: 275–294. doi:10.1006/jtbi.1996.0025.
- Douady, S., and Couder, Y. 1996c. Phyllotaxis as a dynamical self organizing process. Part III: The simulation of the transient regimes of ontogeny. *J. Theor. Biol.* **178**: 295–312. doi:10.1006/jtbi.1996.0026.
- Erickson, R.O., and Sax, K.B. 1956. Elemental growth rate of the primary root of *Zea mays*. *Proc. Am. Philos. Soc.* **100**: 487–498.
- Foley, J.D., van Dam, A., Feiner, S.K., and Hughes, J.F. 1990. Computer graphics, principles and practice. Addison-Wesley, Reading, Mass.
- Green, P.B. 1992. Pattern formation in shoots: a likely role for minimal energy configurations of the tunica. *Int. J. Plant Sci.* **153**: S59–S75. doi:10.1086/297064.
- Hejnowicz, Z., and Romberger, J.A. 1984. Growth tensor of plant organs. *J. Theor. Biol.* **110**: 93–114. doi:10.1016/S0022-5193(84)80017-X.
- Hejnowicz, Z., Nakielski, J., and Hejnowicz, K. 1984. Modeling of spatial variations of growth within apical domes by means of the growth tensor II. Growth specified on dome surface. *Acta Soc. Bot. Pol.* **53**: 301–316.
- Hellendoorn, P.H., and Lindenmayer, A. 1974. Phyllotaxis in *Bryophyllum tubiflorum*: morphogenetic studies and computer simulations. *Acta Bot. Neerl.* **23**: 473–492.
- Hellwig, H., Engelmann, R., and Deussen, O. 2006. Contact pressure models for spiral phyllotaxis and their computer simulation. *J. Theor. Biol.* **240**: 489–500. doi:10.1016/j.jtbi.2005.10.008. PMID:16325204.
- Hofmeister, W. 1868. Allgemeine Morphologie der Gewächse. *In* Handbuch der Physiologischen Botanik. Edited by A.D. Bary, T.H. Irmisch, and J. Sachs. Leipzig, Engelmann, Germany. pp. 405–664.
- Jean, R.V. 1994. Phyllotaxis: a systemic study in plant morphogenesis. Cambridge University Press, Cambridge, UK.
- Jean, R.V., and Barabé, D. 2001. Application of two mathematical models to the Araceae, a family of plants with enigmatic phyllotaxis. *Ann. Bot. (Lond.)*, **88**: 173–186.
- Jönsson, H., Heisler, M.G., Shapiro, B.E., Meyerowitz, E.M., and Mjolsness, E. 2006. An auxin-driven polarized transport model for phyllotaxis. *Proc. Natl. Acad. Sci. U.S.A.* **103**: 1633–1638. doi:10.1073/pnas.0509839103. PMID:16415160.
- Kwiatkowska, D. 1995. Ontogenetic changes of phyllotaxis in *Anagallis arvensis* L. *Acta Soc. Bot. Pol.* **64**: 319–325.
- Kwiatkowska, D. 1997. Intraspecific variation of phyllotaxis in *Anagallis arvensis*. *Acta Soc. Bot. Pol.* **66**: 259–271.
- Kwiatkowska, D. 2006. Flower primordium formation at the *Arabidopsis* shoot apex: quantitative analysis of surface geometry and growth. *J. Exp. Bot.* **57**: 571–580. doi:10.1093/jxb/erj042. PMID:16377735.
- Kwiatkowska, D., and Florek-Marwitz, J. 1999. Ontogenetic variation of phyllotaxis and apex geometry in vegetative shoots of *Sedum maximum* (L.) Hoffm. *Acta Soc. Bot. Pol.* **68**: 85–95.

- Lyndon, R.F. 1998. The shoot apical meristem: its growth and development. Cambridge University Press, Cambridge, UK.
- Meinhardt, H. 1982. Models of biological pattern formation. Academic Press, London, UK.
- Meinhardt, H. 2003. Complex pattern formation by a self-stabilization of established patterns: chemotactic orientation and phyllotaxis as examples. *C.R. Biol.* **326**: 223–237. PMID:12754941.
- Mitchison, G.J. 1977. Phyllotaxis and the Fibonacci series. *Science*, **196**: 270–275. doi:10.1126/science.196.4287.270.
- Nakielski, J. 2000. Tensorial model for growth and cell division in the shoot apex. *In* Pattern formation in biology, vision, and dynamics. Edited by A. Carbone, M. Gromov, and P. Prusinkiewicz. World Scientific, Singapore. pp. 252–267.
- Reinhardt, D., Pesce, E.R., Stieger, P., Mandel, T., Baltensperger, K., Bennett, M., Traas, J., Friml, J., and Kuhlemeier, C. 2003. Regulation of phyllotaxis by polar auxin transport. *Nature*, **426**: 255–260. doi:10.1038/nature02081. PMID:14628043.
- Reinhardt, D., Frenz, M., Mandel, T., and Kuhlemeier, C. 2005. Microsurgical and laser ablation analysis of leaf positioning and dorsoventral patterning in tomato. *Development*, **132**: 15–26. PMID:15563522.
- Richards, O.W., and Kavanagh, A.J. 1943. The analysis of relative growth gradients and changing form of growing organisms: illustrated by the tobacco leaf. *Am. Nat.* **77**: 385–399. doi:10.1086/281140.
- Ridley, J.N. 1982. Packing efficiency in sunflower heads. *Math. Biosci.* **58**: 129–139. doi:10.1016/0025-5564(82)90056-6.
- Schoute, J.C. 1913. Beiträge zur Blattstellungslehre. I. Die Theorie. *Recl Trav. Bot. Neerl.* **10**: 153–339.
- Schwabe, W.W. 1984. Phyllotaxis. *In* Positional control in plant development. Edited by P.W. Barlow and D.J. Carr. Cambridge University Press, Cambridge, UK. pp. 403–440.
- Schwabe, W.W., and Clewer, A.G. 1984. Phyllotaxis — a simple computer model based on the theory of a polarly-translocated inhibitor. *J. Theor. Biol.* **109**: 595–619. doi:10.1016/S0022-5193(84)80161-7.
- Schwendener, S. 1878. Mechanische Theorie der Blattstellungen. Leipzig, Engelmann, Germany.
- Smith, C., Prusinkiewicz, P., and Samavati, F. 2003. Local specification of surface subdivision algorithms. *In* Lecture notes in computer science. Vol. 3062. Springer, Berlin. pp. 313–327.
- Smith, R.S., Guyomarç'h, S., Mandel, T., Reinhardt, D., Kuhlemeier, C., and Prusinkiewicz, P. 2006. A plausible model of phyllotaxis. *Proc. Natl. Acad. Sci. U.S.A.* **103**: 1301–1306.
- Snow, M., and Snow, R. 1931. Experiments on phyllotaxis. I. The effect of isolating a primordium. *Philos. Trans. R. Soc. Lond. B Biol. Sci.* **221**: 1–43.
- Steeves, T.A., and Sussex, I.M. 1989. Patterns in plant development. Cambridge University Press, Cambridge, UK.
- Thornley, J.H.M. 1975. Phyllotaxis I. A mechanistic model. *Ann. Bot. (Lond.)*, **39**: 491–507.
- Turing, A.M. 1952. The chemical basis of morphogenesis. *Philos. Trans. R. Soc. Lond. B Biol. Sci.* **237**: 37–52.
- Veen, A.H., and Lindenmayer, A. 1977. Diffusion mechanism for phyllotaxis, theoretical, physico-chemical and computer study. *Plant Physiol.* **60**: 127–139. PMID:16660024.
- Wardlaw, C.W. 1968. Morphogenesis in plants. Methuen & Co., London, UK.
- Yotsumoto, A. 1993. A diffusion model for phyllotaxis. *J. Theor. Biol.* **162**: 131–151. doi:10.1006/jtbi.1993.1080.
- Young, D.A. 1978. On the diffusion theory of phyllotaxis. *J. Theor. Biol.* **71**: 421–432. doi:10.1016/0022-5193(78)90169-8. PMID:642539.
- Zagórska-Marek, B. 1985. Phyllotactic patterns and transitions and transitions in *Abies balsamea*. *Can. J. Bot.* **63**: 1844–1854.
- Zagórska-Marek, B. 1994. Phyllotactic diversity in *Magnolia* flowers. *Acta Soc. Bot. Pol.* **63**: 117–137.

Appendix A

Appendix appears on the following page.

Table A1. Parameter values for simulations used in the figures and videos.

Parameter	Symbol	Eq.	Fig. 5; Video 15117	Fig. 6	Figs. 7 and 8	Fig. 9; Table 1	Fig. 10	Fig. 12a
Time step			0.005	0.12	0.1	0.01	0.01	0.1
Active ring sampling points		5, 6, 7	480	100	38	500	120	60
Active ring position			0.08	0.06	0.08	0.06	0.02	0.04
Horizontal noise			0	0	0	0	0	0
Vertical noise			0	0	0	0	0	0
Inhibition function model			Single	Single	Single	Single	Single	Double
Initial whorls*			2	1	1	20, 10	5	1
Initial primordia per whorl*			1	1	1	1, 2	2	1
Initial angle (°)*						77.96, 99.50, 106.4, 137.51, 151.14, 68.76	68.76	
Long threshold [†]			1.5, 52.5	0.32, 1.6, 0.48	5.4	180	120	0.42
Long range inhibition exponent of time	b_l	5, 6	1	1	1	1.1	1.1	1.1
Short threshold								8.3
Short range inhibition exponent of time	b_s	7						4
Long range delay exponent of time	b_d	6						1.6

Note: The videos are available as supplementary data.

*Multiple values given for the simulations in Fig. 9 and Table 1. See Fig. 9 legend for details.

[†]Multiple values given for simulations that vary the long-range inhibition threshold during simulation to effect a transition in phyllotaxis type or order.

Fig. 12b	Fig. 12c	Fig. 12d	Fig. 12e	Fig. 12f	Fig. 12g	Fig. 13a	Fig. 13b	Fig. 14	Video 25117
0.1	0.1	0.1	0.05	0.1	0.1	0.2	0.2	0.3	0.02
60	60	60	60	80	80	60	60	60	480
0.04	0.04	0.04	0.01	0.01	0.02	0.04	0.04	0.04	0.08
0	0	0	0	0	0	0	0	0.05	0
0	0	0	0	0	0	0	0	0.005	0
Double	Double	Double							
1	1	3	2	3	3	1	1	1	1
2	2	1	1	1	2	2	2	2	2
			150	99.5	68.75				
4.2	5.3	4.2	170	170	40	4, 20	4, 20	1.25	2.5, 10.5
1.1	1.1	1.1	1.1	1.1	1.1	1.1	1.1	1.1	1
25	13	33	15	30	60	20, 2.4	20	12.5	14
4	4	4	4	4	4	4	4	4	4
1.6	1.6	1.6	1.6	1.6	1.6	1.6	1.6	1.6	1.6